FMCW Waveform Design With Good Correlation Level for the Joint Radar and Communications

Yuhan Wang, Yongzhe Li and Ran Tao
School of Information and Electronics, Beijing Institute of Technology, Beijing 100081, China
Emails: yuhan.wang@bit.edu.cn, lyz@ieee.org/yongzhe.li@bit.edu.cn, rantao@bit.edu.cn

***Abstract*—In this paper, we propose frequency modulated continuous wave (FMCW) design and receive processing techniques for joint radar and communications. Our approach simultaneously takes into account the correlation property of waveform and interference mitigation for radar while enabling information embedding (IE) for communications. Specifically, we adopt an advanced IE strategy using hybrid modulations to enhance communication rates. Meanwhile, we seek to minimize the integrated sidelobe level of FMCW waveform to optimize the correlation level and leverage waveform agility to mitigate interference for radar. The design leads to a non-convex optimization problem. To address it, we choose to directly manipulate the polynomial coefficients in the phase elements of FMCW waveform and reformulate it into a proper form. We then make use of the majorization-minimization technique to find solutions through iterations for solving the reformulated design. A closed-form solution is obtained at each iteration. Our major contribution also lies in proposing a demodulation method for communications. Simulation results verify the effectiveness of the proposed FMCW design and its superiority over existing work.**

***Index Terms*—Frequency modulated continuous wave, information embedding, integrated sidelobe level, interference mitigation, waveform design.**

I. Introduction

The joint radar and communications (JRC) [1], which aims to tackle the issues of radio-frequency spectrum congestion, has attracted significant interest over the past decade. Driven by continuous advancements in research, JRC has emerged as a key technology for autonomous driving, enabling real-time sensing and reliable vehicle-to-vehicle communication [2]–[4]. Moreover, JRC systems offer many benefits for autonomous vehicles, including reduced hardware costs [2], enhanced energy efficiency [3], improved interference management [4], and so on. These features make JRC to become an essential technology for the future of autonomous vehicles.

In the autonomous driving JRC system, one of the most popular waveforms is the frequency modulated continuous wave (FMCW). The FMCW enables high resolution and strong robustness from the perspective of radar. For communications in JRC, a proper information embedding (IE) strategy to improve the communication rate is also of importance. To this end, different modulation methods have been experimented to conduct IE for the JRC. For example, some studies employ phase shift keying (PSK) [5], quadrature amplitude modulation [6], or frequency shift keying (FSK) [7] to embed communication information into each chirp signal of FMCW. Although these single-modulation based IE methods can be easily implemented, they typically lead to low communication rates and increased bandwidth requirements. These motivate us to develop new IE strategies to improve the communication rate of FMCW-driven JRC.

When it comes to the radar performance of the FMCW based JRC, the correlation property of the FMCW waveform is crucial for the receiver to estimate range and velocity information of targets. There exist some studies that achieve good correlation properties from the perspective of integrated sidelobe level (ISL) minimization [8]–[10]. For example, the algorithms such as 'CAN' [8], 'MM-Corr' [9], and 'ISLNew' [10] have been used to design waveforms with good ISL performance. However, these works mainly focus on phase-coded waveforms. Normally, they cannot be direct used for FMCW. This inspires us to consider the ISL performance when designing FMCW waveform.

Another important factor that affects the radar performance of JRC is the mutual interference among FMCW radars, especially the coherent interference [11]–[13]. It is generated when the interference radar and victim radar have the same chirp rate. It creates ghost targets during range-Doppler (RD) estimation, which can cause false alarms. Some existing studies have addressed this issue through transmit waveform design, such as frequency hopping [14] and phase coding [15]. The main idea therein is to design the waveform agility, so that the transmit waveform and the interference have different signal forms. This ensures that the interference is dispersed to different frequency units after mixing, thereby avoiding confusion between the interference and the true targets. However, these works consider either radar or communication function only. This motivates us to design dual-function FMCW while mitigating the coherent interference.

In this paper, we focus on the FMCW waveform design for the autonomous driving JRC. Our goal is to reduce the ISL of FMCW waveform for radar and meanwhile to conduct IE for communications. Moreover, we also aim to mitigate coherent interference among FMCW radars. To this end, we exploit the diversities of phase, frequency, and chirp rate of the FMCW waveform to fulfill the goal of reducing the ISL and implementing the IE. We formulated the design as a nonconvex optimization problem, which is solved through majorization-minimization (MM) techniques. The interference is effectively mitigated by exploiting the agility of the FMCW waveform. In addition, we propose a method to demodulate communication information embedded by hybrid modulations. Finally, we

This work was supported in part by the National Natural Science Foundation of China (NSFC) under grants 62271054 and U21A20456.

provide simulations to verify the effectiveness of our design.

Notations: We use $\otimes$, $\odot$, $|\cdot|$, $\lfloor\cdot\rfloor$, $(\cdot)^{\mathrm{T}}$, $(\cdot)^{\mathrm{H}}$, ∇, ∇^2, $\mathrm{Re}\{\cdot\}$, $\mathrm{Im}\{\cdot\}$, $\lambda_{\max}\{\cdot\}$ to denote the Kronecker product, Hadamard product, modulus, floor function, transpose, Hermitian transpose, gradient, Hessian, real part, imaginary part, and the largest eigenvalue of a matrix, respectively. Moreover, operators $\mathcal{V}(\cdot)$, $\mathfrak{D}\{\cdot\}$, $\mathcal{F}_Q\{\cdot\}$, $\mathcal{G}_Q\{\cdot\}$, and $\mathcal{T}\{\cdot\}$ denote forming a vandermonde matrix, forming a diagonal matrix whose main diagonal entries are picked up from the input vector, applying the $(2Q-1)$-point fast Fourier transform (FFT), picking up the first Q elements to form a new vector, and constructing a Hermitian Toeplitz matrix whose first column coincides with the input vector, repectively. In addition, $e^{j(\cdot)}$ denote the exponential functions that is applied to the argument elementwisely, $\mathbf{1}_M$ stands for an $M\times 1$ vector with all elements equal to 1, and $\mathbf{I}_M$ is the $M\times M$ identity matrix.

II. Signal Model

Consider a JRC vehicle that simultaneously performs functions of radar and communications. The JRC vehicle transmits an FMCW waveform containing L chirp signals. We divide each chirp signal evenly into D subchirp signals in the time domain, and the period and bandwidth of each subchirp are denoted as T_c and B_c, respectively. Thus, the baseband FMCW signal can be expressed as

$$s(t)=\sum_{l=0}^{L-1}\sum_{d=0}^{D-1}\exp\Bigg\{j\Big(\phi_{d,l}+2\pi\big(f_{d,l}(t-(lD+d)T_c) +\frac{1}{2}k_{d,l}(t-(lD+d)T_c)^2\big)\Big)\Bigg\}\mathrm{rect}\left(\tfrac{t-(lD+d)T_c}{T_c}\right) \quad (1)$$

where $\phi_{d,l}$, $f_{d,l}$, and $k_{d,l}$ are the initial phase, initial frequency, and the slope of the d-th subchirp within the l-th chirp signal, respectively, and $\mathrm{rect}(\cdot)$ is a window function which equals 1 only if the argument falls within $[0,T_c)$ and otherwise is 0.

Based on the above model, we have in total $M=LD$ subchirps. With T_{s} being the sampling interval, after sampling P points in a subchirp, the m-th subchirp signal can be expressed as the discrete form given by $\mathbf{x}_m \triangleq [s(t)|_{t=T_{\mathrm{s}}}, s(t)|_{t=2T_{\mathrm{s}}}, ..., s(t)|_{t=PT_{\mathrm{s}}}]^{\mathrm{T}} \in \mathbb{C}^{P\times 1}$, whose p-th element can be expressed as

$$\mathbf{x}_m(p)=e^{j(\alpha_m+\beta_m p+\gamma_m p^2)} \quad (2)$$

where $\alpha_m \triangleq \phi_m$, $\beta_m \triangleq 2\pi f_m T_s$, and $\gamma_m \triangleq \pi k_m T_s^2$ are the phase coefficients of the m-th subchirp signal, which are related to ϕ_m, f_m and k_m, respectively.

Let us define $\mathbf{u} \triangleq [1,2,...,P]^{\mathrm{T}} \in \mathbb{N}_+^{P\times 1}$ and $\mathbf{U} \triangleq \mathcal{V}(\mathbf{u})\tilde{\mathbf{I}} \in \mathbb{N}_+^{P\times 3}$ as the sampling vector and sampling matrix, respectively. Moreover, we introduce the vector $\boldsymbol{\gamma}_m \triangleq [\alpha_m,\beta_m,\gamma_m]^{\mathrm{T}} \in \mathbb{R}^{3\times 1}$, which contains three phase coefficients of the m-th subchirp signal. After that, we can rewrite $\mathbf{x}_m$ as

$$\mathbf{x}_m = e^{j(\mathbf{U}\boldsymbol{\gamma}_m)} \quad (3)$$

Stacking all the $Q \triangleq MP$ elements $\{\mathbf{x}_m(p)\}_{m,p}^{M,P}$ into a vector, we can get

$$\mathbf{x}=e^{j((\mathbf{I}_M\otimes\mathbf{U})\mathbf{z})} \quad (4)$$

where the vector $\mathbf{z} \triangleq \left[\boldsymbol{\gamma}_1^{\mathrm{T}},\boldsymbol{\gamma}_2^{\mathrm{T}},\cdots,\boldsymbol{\gamma}_M^{\mathrm{T}}\right]^{\mathrm{T}} \in \mathbb{R}^{3M\times 1}$ is composed of phase coefficients of all chirp signals.

The vector $\mathbf{x}$ is expected to have good correlation property, thereby enhancing the good extraction of targets. Toward this end, the ISL that characterizes the accumulated sidelobes of the waveform is typically used, which can be expressed as

$$\zeta \triangleq \sum_{\substack{q=-Q+1\\ q\neq 0}}^{Q-1}|r(q)|^2 \quad (5)$$

where $r(q) \triangleq \sum_{n=q+1}^{Q-1}x(n)x^*(n-q) = r^*(-q), \forall q \in \{0,\ldots,Q-1\}$ denotes the auto-correlations of the waveform vector $\mathbf{x}$ at all time lags.

III. The FMCW Waveform Design With IE

To address the issue of low-speed transmission rate of FMCW, we apply the hybrid modulations to implement IE. Our idea here is to simultaneously apply the index modulation (IM), PSK modulation, and FSK modulation to the subchirps of FMCW. To be specific, we partially choose D_{c} ($D_{\mathrm{c}} \le D$) subchirps from the D subchirps within each chirp with IM to transmit symbols. We then respectively adopt PSK and FSK modulations to embed communication information into the initial phases and the initial frequencies. The slopes are fixed at $k=B_{\mathrm{c}}/T_{\mathrm{c}}$ for the chosen D_{c} subchirp signals.

In order to establish a relationship between the transmitted communication symbols and the phase coefficient vector $\mathbf{z}$, we first introduce an index vector, denoted by $\mathbf{v}\in\mathbb{R}^{3M\times 1}$, to record the indices of the subchirps chosen for IE. Note that for the indices selected for IE, the corresponding elements of the index vector $\mathbf{v}$ are set to 1, while the elements of the index vector $\mathbf{v}$ for the unselected indices are set to 0. We then define $\mathbf{z}_{\mathrm{c}} \in \mathbb{R}^{3M\times 1}$ as the predetermined coefficient vector, which contains the phase coefficients for IE at the positions indexed by $\mathbf{v}$ while otherwise enable zero elements. Depending on the mapping rule of user choice, the phase coefficients of the subchirps selected for IE are mapped to the phase coefficient vector $\mathbf{z}$, which can be expressed as $\mathbf{z}_{\mathrm{c}}=\mathbf{z}\odot\mathbf{v}$. Based on this, we successfully establish the relationship between the communication symbols and the phase coefficients of the transmit signals. For example, when the n-th phase coefficient of the m-th subchirp is chosen to carry communication information, then the relationship $\mathbf{z}(3(m-1)+n)=\mathbf{z}_{\mathrm{c}}(3(m-1)+n), \forall m \in \{1,\ldots,M\}, n\in\{1,2,3\}$ holds.

Among all possible mapping rules for the IE studied here, the maximal embeddable bits per chirp, denoted by $R_{\max}$, can be given as follows

$$R_{\max}=\left\lfloor D_{\mathrm{c}}\log_2(DN)+\log_2\frac{D!}{D_{\mathrm{c}}!(D-D_{\mathrm{c}})!}\right\rfloor \quad (6)$$

where N denotes the number of all possible symbols associated with PSK modulation. The former summing component

is determined by the PSK modulation and FSK modulation involved in the IE, and the latter is additionally introduced by the aforementioned IM. We omit the derivation of (6) due to the space limitation.

Based on the IE strategy proposed above, we further consider to reduce the ISL of FMCW. To this end, the FMCW waveform design problem under both considerations on the IE and ISL minimization can be formulated as follows

$$\min_{\mathbf{x},\mathbf{z}} \quad \zeta \tag{7a}$$

$$\text{s.t.} \quad \mathbf{z} \odot \mathbf{v} = \mathbf{z}_{\mathrm{c}} \tag{7b}$$

$$\mathbf{x} = e^{j((\mathbf{I}_M \otimes \mathbf{U})\mathbf{z})} \tag{7c}$$

where the ISL ζ in the objective function has been defined in (5). Note that the constraint (7b) results from the previously proposed IE strategy with $\mathbf{z}_{\mathrm{c}}$ predetermined by our symbol mapping rule, and (7c) results from (4).

Before proceeding with (7), we need to derive the ISL ζ into a proper form, so that the problem (7) can be tackled. To this end, we transform the ISL ζ in (5) into frequency domain which can be derived as the following form

$$\begin{aligned}\zeta =& \frac{1}{2Q}\sum_{q=1}^{2Q}\left(\left((e^{j((\mathbf{I}_M\otimes\mathbf{U})\mathbf{z})})^{\mathrm{H}}\mathbf{a}_q\mathbf{a}_q^{\mathrm{H}}e^{j((\mathbf{I}_M\otimes\mathbf{U})\mathbf{z})}\right)^2\right.\\ &\left.-2Q\left((e^{j((\mathbf{I}_M\otimes\mathbf{U})\mathbf{z})})^{\mathrm{H}}\mathbf{a}_q\mathbf{a}_q^{\mathrm{H}}e^{j((\mathbf{I}_M\otimes\mathbf{U})\mathbf{z})}\right)+Q^2\right)\end{aligned} \tag{8}$$

where $\mathbf{a}_q \triangleq [1,\ e^{j\omega_q},\ \ldots,\ e^{j(Q-1)\omega_q}]^{\mathrm{T}}$ with $\omega_q = \frac{2\pi}{2Q}q$. The last two sum terms of (8) are constant, which are immaterial to optimization. After ignoring them, the problem (7) can be rewritten as

$$\min_{\mathbf{z}} \quad \frac{1}{2Q}\sum_{q=1}^{2Q}\left((e^{j((\mathbf{I}_M\otimes\mathbf{U})\mathbf{z})})^{\mathrm{H}}\mathbf{a}_q\mathbf{a}_q^{\mathrm{H}}e^{j((\mathbf{I}_M\otimes\mathbf{U})\mathbf{z})}\right)^2 \tag{9a}$$

$$\text{s.t.} \quad \mathbf{z} \odot \mathbf{v} = \mathbf{z}_{\mathrm{c}} \tag{9b}$$

which is a nonconvex optimization problem with respect to $\mathbf{z}$.

In order to solve (9), we make use of the majorization-minimization technique. Before dealing with (9), we present the following result (see Lemma 1 of [10]).

Lemma 1. *If a real-valued function $f(\mathbf{x})$ with a real variable $\mathbf{x}$ is second-order differentiable, and there is a matrix $\mathbf{G}$ satisfying the generalized inequality $\nabla^2 f(\mathbf{x}) \preceq \mathbf{G}$ for all $\mathbf{x}$. For each point $\mathbf{x}_0$, the following convex quadratic function*

$$g(\mathbf{x}) = f(\mathbf{x}_0)+\nabla f(\mathbf{x}_0)^{\mathrm{T}}(\mathbf{x}-\mathbf{x}_0)+\frac{1}{2}(\mathbf{x}-\mathbf{x}_0)^{T}\mathbf{G}(\mathbf{x}-\mathbf{x}_0) \tag{10}$$

majorizes $f(\mathbf{x})$ at $\mathbf{x}_0$.

To find a proper majorization function for the objective of (9) (denoted hereafter as $f(\mathbf{z})$) via Lemma 1, the first-order gradient of $f(\mathbf{z})$ (i.e., $\nabla f(\mathbf{z})$) and the matrix $\mathbf{G}$ that satisfies $\nabla^2 f(\mathbf{z}) \preceq \mathbf{G}$ have to be both available.

Introducing the matrix $\mathbf{A} \triangleq [\mathbf{a}_1, \mathbf{a}_2, ..., \mathbf{a}_{2Q}]^{\mathrm{H}}$, after some derivations, we obtain the first-order gradient of $f(\mathbf{z})$, i.e.,

$$\begin{aligned}\nabla f(\mathbf{z}) = \frac{2}{Q}\,\mathrm{Im}\Big\{\Big((\mathbf{I}_M\otimes\mathbf{U})^{\mathrm{H}}(\mathcal{T}\{\mathbf{A}^{\mathrm{H}}|\mathbf{A}e^{j((\mathbf{I}_M\otimes\mathbf{U})\mathbf{z})}|^2\}\\ e^{j((\mathbf{I}_M\otimes\mathbf{U})\mathbf{z})}\Big)\odot\Big((\mathbf{I}_M\otimes\mathbf{U})^{\mathrm{H}}e^{-j((\mathbf{I}_M\otimes\mathbf{U})\mathbf{z})}\Big)\Big\}.\end{aligned} \tag{11}$$

To simplify the expression, we introduce the vector $\mathbf{z}' \triangleq (\mathbf{I}_M \otimes \mathbf{U})\mathbf{z}$ here. We can then obtain $\nabla^2 f(\mathbf{z})$ as follows

$$\begin{aligned}\nabla^2 f(\mathbf{z}) =& \frac{2}{Q}\sum_{q=1}^{2Q}\Big(\mathrm{Im}\{(\mathbf{I}_M\otimes\mathbf{U})^{\mathrm{H}}(\mathbf{A}_p\mathbf{A}_p^{\mathrm{H}}e^{j\mathbf{z}'})\odot(\mathbf{I}_M\otimes\mathbf{U})^{\mathrm{H}}e^{-j\mathbf{z}'}\}\\ &\times\mathrm{Im}\Big\{(\mathbf{I}_M\otimes\mathbf{U})^{\mathrm{H}}(\mathbf{A}_p\mathbf{A}_p^{\mathrm{H}}e^{j\mathbf{z}'})\odot((\mathbf{I}_M\otimes\mathbf{U})^{\mathrm{H}}e^{-j\mathbf{z}'})\Big\}^{\mathrm{T}}\\ &+|\mathbf{A}_p^{\mathrm{H}}e^{j\mathbf{z}'}|^2\mathrm{Re}\Big\{(\mathbf{I}_M\otimes\mathbf{U})^{\mathrm{H}}\mathfrak{D}\{e^{j\mathbf{z}'}\}\mathbf{A}_p\mathbf{A}_p^{\mathrm{H}}\mathfrak{D}\{e^{-j\mathbf{z}'}\}(\mathbf{I}_M\otimes\mathbf{U})\Big\}\Big)\\ &-\mathrm{Re}\Big\{\mathfrak{D}\Big\{(\mathbf{I}_M\otimes\mathbf{U})^{\mathrm{H}}\mathcal{T}\{\mathbf{A}^{\mathrm{H}}|\mathbf{A}e^{j\mathbf{z}'}|^2\}e^{j\mathbf{z}'}\odot(\mathbf{I}_M\otimes\mathbf{U})^{\mathrm{H}}e^{-j\mathbf{z}'}\Big\}\Big\}.\end{aligned} \tag{12}$$

For the selection of $\mathbf{G}$, the generalized inequality $\mathbf{G} \succeq \nabla^2 f(\mathbf{z})$ holds if $\mathbf{G}$ is designed as $\mathbf{G} \triangleq \lambda\mathbf{I}_{\mathrm{Q}}$, where λ is a constant that can take the largest eigenvalue of $\nabla^2 f(\mathbf{z})$. We omit derivations to (11) and (12) due to the space limitation and refer readers to [16].

Based on the expression (11) and (12), the majorization function for the optimization problem (9) can be written as

$$\begin{aligned}g(\mathbf{z},\mathbf{z}^{(k)}) =& \Big(\frac{2}{Q}\mathrm{Im}\Big\{\Big((\mathbf{I}_M\otimes\mathbf{U})^{\mathrm{H}}(\mathcal{T}\{\mathbf{A}^{\mathrm{H}}|\mathbf{A}e^{j((\mathbf{I}_M\otimes\mathbf{U})\mathbf{z}^{(k)})}|^2\})\\ &e^{j((\mathbf{I}_M\otimes\mathbf{U})\mathbf{z}^{(k)})}\Big)\odot\Big((\mathbf{I}_M\otimes\mathbf{U})^{\mathrm{H}}e^{-j((\mathbf{I}_M\otimes\mathbf{U})\mathbf{z}^{(k)})}\Big)\Big\}\\ &-\lambda\mathbf{z}^{(k)}\Big)^{\mathrm{T}}\mathbf{z}+\frac{\lambda}{2}\mathbf{z}^{\mathrm{T}}\mathbf{z}+\text{const}\end{aligned} \tag{13}$$

where $\mathbf{z}^{(k)}$ is obtained at the k-th iteration. Ignoring constant terms in (13), we can rewrite the optimization problem (9) as

$$\begin{aligned}\min_{\mathbf{z}}\ \Big(&\frac{2}{Q}\mathrm{Im}\Big\{\Big((\mathbf{I}_M\otimes\mathbf{U})^{\mathrm{H}}(\mathcal{T}\{\mathbf{A}^{\mathrm{H}}|\mathbf{A}e^{j((\mathbf{I}_M\otimes\mathbf{U})\mathbf{z}^{(k)})}|^2\})\\ &e^{j((\mathbf{I}_M\otimes\mathbf{U})\mathbf{z}^{(k)})}\Big)\odot\Big((\mathbf{I}_M\otimes\mathbf{U})^{\mathrm{H}}e^{-j((\mathbf{I}_M\otimes\mathbf{U})\mathbf{z}^{(k)})}\Big)\Big\}\\ &-\lambda\mathbf{z}^{(k)}\Big)^{\mathrm{T}}\mathbf{z}+\frac{\lambda}{2}\mathbf{z}^{\mathrm{T}}\mathbf{z}\end{aligned} \tag{14a}$$

$$\text{s.t.} \quad \mathbf{z} \odot \mathbf{v} = \mathbf{z}_{\mathrm{c}} \tag{14b}$$

whose closed-form solution at the k-th iteration is

$$\mathbf{z} = \mathbf{z}_{\mathrm{c}} + (\mathbf{1}_{3M} - \mathbf{v}) \odot \mathbf{b}^{(k)} \tag{15}$$

with

$$\begin{aligned}\mathbf{b}^{(k)} \triangleq \mathbf{z}^{(k)} - &\frac{4}{\lambda}\mathrm{Im}\Big\{\Big((\mathbf{I}_M\otimes\mathbf{U})^{\mathrm{H}}\mathcal{G}_Q\{\mathcal{F}_Q^{-1}\{\mathcal{F}_Q\{e^{j((\mathbf{I}_M\otimes\mathbf{U})\mathbf{z}^{(k)})}\}\}\\ \odot&\Big|\mathcal{F}_Q\{e^{j((\mathbf{I}_M\otimes\mathbf{U})\mathbf{z}^{(k)})}\}\Big|^2\}\Big)\odot\Big((\mathbf{I}_M\otimes\mathbf{U})^{\mathrm{H}}e^{-j((\mathbf{I}_M\otimes\mathbf{U})\mathbf{z}^{(k)})}\Big)\Big\}.\end{aligned}$$

IV. Receive Processing Design

In this section, we first show the target RD estimation method of radar receiver, and then propose an information demodulation method for communication receiver.

For Radar Range-Doppler Estimation: Since multiple short subchirps are used in this paper, the two-dimensional FFT method of traditional FMCW radar cannot be used directly for RD estimation. Therefore, we use the parameter matching method to estimate the range and velocity of the target which has been shown in [7].

TABLE I: Performance comparisons of the tested algorithms versus numbers of available subchirps.

	$D=8$				$D=12$				$D=16$				$D=20$				$D=24$			
	Min.[a]	Ave.[b]	Iter.[c]	Time[d]	Min.	Ave.	Iter.	Time	Min.	Ave.	Iter.	Time	Min.	Ave.	Iter.	Time	Min.	Ave.	Iter.	Time
PECS	42.05	42.93	19439	176.249	46.08	46.69	23387	205.773	48.28	48.89	34266	258.341	51.07	52.31	46813	298.740	52.94	54.14	82179	707.728
Proposed	37.94	38.50	836	0.658	40.98	41.45	1076	2.319	43.17	43.64	1188	3.867	45.02	45.43	1342	6.918	46.38	46.80	2527	17.230

[a]Min.: Minimum ISL value (in dB). [b]Ave.: Average ISL value (in dB). [c]Iter.: Average number of iteration numbers. [d]Time: Average time consumption (in seconds).

TABLE II: Performance comparison between two strategies.

	$R_{\max}$=18	$R_{\max}$=42	$R_{\max}$=48	$R_{\max}$=78	$R_{\max}$=90
PSK+FSK	44.80 dB	51.23 dB	53.57 dB	59.13 dB	60.83 dB
Proposed	43.86 dB	46.95 dB	48.85 dB	57.16 dB	60.17 dB

For Communication Demodulation Design: To detect subchirps that are used for IE and to demodulate the phase and frequency information corresponding to PSK and FSK modulations, we propose a joint demodulation (JD) method. Based on the reference signal model $s_d(t;r)=e^{j2\pi(f_r t+\frac{B_c}{2T_c}t^2)}$, the mixed signal can be obtained by multiplying the i-th receive signal with the conjugation of the r-th reference signal. We denote f_s^{com} as the Nyquist sampling rate. After sampling the mixed signal, the p-th sample can be expressed as

$$y(p)=he^{j\phi_i}e^{j2\pi(f_i-f_r)pT_s^{\text{com}}}e^{j\pi(k_i-\frac{B_c}{T_c})(pT_s^{\text{com}})^2}+w(p) \quad (16)$$

where $0\le i\le LD-1$, $0\le r\le D-1$, $0\le p\le P_s$, and $T_s^{\text{com}}=1/f_s^{\text{com}}$ and P_s are the sampling interval and the total number of samples of a subchirp, respectively. In addition, h is the rayleigh fading coefficient, $f_r\in\mathcal{D}$ indicates the frequency information of the reference signal, $\mathcal{D}$ is the optional set of FSK for IE, and $w(p)$ is the additive white gaussian noise.

For the IE strategy we devised, when the i-th subchirp is used for communications, its chirp rate is $k_i=B_c/T_c$. Based on this, we apply the maximum likelihood principle to jointly detect the phase and frequency information corresponding to PSK and FSK modulations, which can be expressed as

$$(f_i^*,\phi_i^*)=\arg\min_{f_r\in\mathcal{D},\phi_r\in\mathcal{N}}\left|\frac{1}{P_s}\sum_{p=0}^{P_s-1}y(p)-h_ie^{j\phi_r}\right|^2 \quad (17)$$

where $\phi_r\in\mathcal{N}$ indicates the phase information of the reference signal, $\mathcal{N}$ is the optional set of PSK for IE, and f_i^* and ϕ_i^* are the detected frequency and phase, respectively.

Since the receiver knows the number of subchirps used for communication, i.e., D_c, we can take D subchirps as a group to find the D_c subchirps with the lowest energy in each group, and demodulate communication information.

V. Simulation Results

We first compare the performances of our proposed algorithm with those of the existing method 'PECS' in [17]. Then, we evaluate the performances of our proposed IE strategy associated with PSK, FSK and IM, and compare it to the method in [7] that solely involves PSK and FSK modulations, followed by some evaluations on interference mitigation and communication performances. Throughout simulations, we set the number of chirp signals as $L=4$. For the PSK modulation used in simulations, we always choose the quadrature phase shift keying scheme for evaluations. Moreover, we choose the absolute difference of the ISL values obtained at the current and previous iterations normalized by the initial ones as the stopping criterion, whose tolerance is set to be 10^{-7}.

In the first example, we compare our proposed algorithm with 'PECS', wherein the number of available subchirp signals D ranges within $[8,24]$ with uniform intervals spacing 4. For all tested algorithms, the number of chosen subchirps for IE is set to be $D_c=1$. The corresponding results are shown in Table 1, which are obtained over 30 independent trials. It can be seen from Table 1 that our proposed algorithm outperforms 'PECS' for all tested cases. For example, in the case of $D=16$, the ISL optimized by the algorithm we proposed is approximately 6 dB lower than that optimized by the 'PECS' algorithm. In addition, our proposed algorithm costs less time consumption and fewer iterations than those of 'PECS'. This example verifies the superiority of our proposed algorithm on optimization effect and convergence speed.

In the second example, we compare our proposed IE scheme associated with PSK, FSK, and IM modulations to the method in [7] with PSK and FSK modulations only. Different scenarios versus varying $R_{\max}$ chosen from the set $\{18,42,48,78,90\}$ are tested. Other parameters include $D=16$ and $N=4$. In order to reach the above maximal embeddable bits per chirp, our proposed IE strategy and the IE strategy in [7] require selecting D_c subchirps for IE within each chirp, which can be chosen from $\{2,5,6,11,14\}$ and $\{3,7,8,13,15\}$, respectively (see (6) and the explanations therein). The corresponding results are shown in Table 2, which are obtained over 30 independent trials. It can be seen from Table 2 that the FMCW associated with our proposed IE strategy shows lower ISL values than that of the IE strategy in [7] when the same $R_{\max}$ is achieved, for all tests. For example, in the case of $R_{\max}=48$, according to the proposed IE strategy, we need to select 6 subchirps within each chirp for IE and the remaining 10 subchirps for optimizing ISL, while the IE strategy in [7] requires 8 subchirps for IE and the remaining 8 subchirps for optimization. Therefore, based on our proposed IE strategy, the ISL value is reduced around 5 dB lower than that of [7].

In the third example, we compare the radar detection performance of our designed FMCW waveform with that of conventional FMCW in the presence of the coherent interference. Both the signal-to-noise ratio (SNR) and the signal-to-interference ratio are set to 0 dB. The ranges and radial velocities of the two true targets are $\{40\,\text{m},60\,\text{m}\}$ and $\{5\,\text{m/s},10\,\text{m/s}\}$, respectively. The conventional FMCW applies the 2D-FFT processing method [18], while the designed FMCW applies the parameter matching processing method [7].

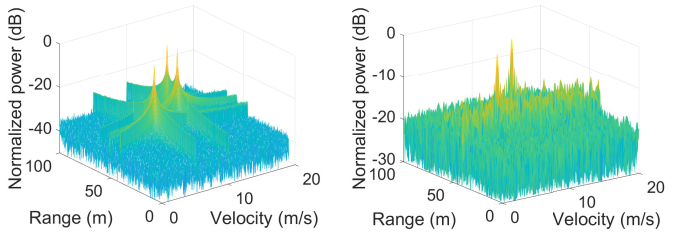

(a) Range-velocity estimation of the conventional FMCW.

(b) Range-velocity estimation of the designed FMCW.

Fig. 1: Evaluations on radar performances.

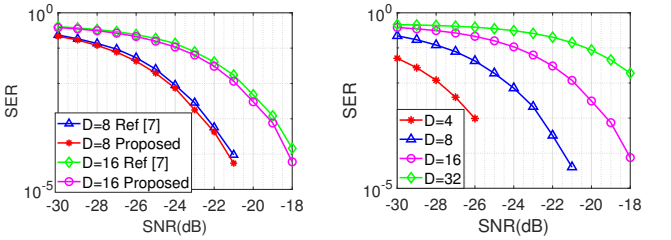

(a) The SER performance evaluations of two demodulation methods.

(b) The SER performance evaluations versus different SNR values.

Fig. 2: Evaluations on communication performances.

After receive processing, the range and velocity estimation results of the targets can be obtained, as shown in Fig. 1. It can be seen from Fig. 1(a) that the conventional FMCW shows three peaks, one of which corresponds to a ghost target caused by interference. Nevertheless, as shown in Fig. 1(b), adopting the designed FMCW can purely detect the two true targets. This improvement is attributed to the high agility of the designed waveform parameters, which reduces the similarity between the interference and the transmit waveform. As a result, the interference signal is effectively prevented from being misidentified as a ghost target during matched filtering. However, this method may lead to an increased sidelobe level.

In the forth example, we compare the symbol error rate (SER) performance of the proposed demodulation method with that of the method in [7], and meanwhile, we evaluate the SER performance versus SNR values. Here, we set $D_c = 4$ for the evaluations with 1000 Monte Carlo experiments. The corresponding results are shown in the two subfigures of Fig. 2. It can be seen from Fig. 2(a) that the proposed JD method can achieve a lower SER than that of the method in [7]. This is because the JD method can solve the problem of error propagation existing in [7], and significantly improve the accuracy of information demodulation. In addition, as shown in Fig. 2(b), it can be seen that the SER values decrease when the tested SNR values increase. Moreover, the case associated with the smallest D shows the best overall SER performances. This example verifies the effectiveness of our proposed IE strategy and demodulation method from the perspective of communications.

VI. Conclusion

We have proposed an efficient FMCW waveform design with good correlation property for the JRC, for which an associated IE strategy has also been proposed. Specifically, we have adopted an advanced IE strategy using hybrid modulations to enhance communication rates. Meanwhile, we have minimized the ISL of the FMCW to improve the waveform correlation for radar, and we have leveraged waveform agility to mitigate interference. The design has been formulated as a non-convex optimization problem, which has been solved by majorization-minimization technique to find solutions through iterations. In addition, we have proposed a method to demodulate information embedded by hybrid modulations. Simulation results have verified the effectiveness of our proposed FMCW design and its superiority over existing work.

References

[1] A. Hassanien, M. G. Amin, E. Aboutanios, and B. Himed, "Dual-function radar communication systems: A solution to the spectrum congestion problem," *IEEE Signal Process Mag.*, vol. 36, no. 5, pp. 115–126, Sep. 2019.

[2] C. Aydogdu, N. Garcia, L. Hammarstrand, and H. Wymeersch, "Radar communications for combating mutual interference of fmcw radars," in *Proc. IEEE Radar Conf. (RadarConf)*, 2019, pp. 1–6.

[3] C. Aydogdu, M. F. Keskin, and H. Wymeersch, "Automotive radar interference mitigation via multi-hop cooperative radar communications," in *Proc. 17th Eur. Radar Conf. (EuRAD)*, 2021, pp. 270–273.

[4] C. Aydogdu, M. F. Keskin, N. Garcia, H. Wymeersch, and D. W. Bliss, "Radchat: Spectrum sharing for automotive radar interference mitigation," *IEEE Trans. Intell. Transp. Syst.*, vol. 22, no. 1, pp. 416–429, 2019.

[5] J. Jung, S. Lim, S.-C. Kim, and S. Lee, "Solving doppler-angle ambiguity of bpsk-mimo fmcw radar system," *IEEE Access*, vol. 9, pp. 120 347–120 357, 2021.

[6] Q. Shi, T. Zhang, X. Yu, X. Liu, and I. Lee, "Waveform designs for joint radar-communication systems with oqam-ofdm," *Signal Process.*, vol. 195, p. 108462, 2022.

[7] M.-X. Gu, M.-C. Lee, and T.-S. Lee, "A novel frequency hopping-aided fmcw integrated radar and communication system," in *Proc. IEEE VTS APWCS*, Aug 2022, pp. 11–15.

[8] H. He, P. Stoica, and J. Li, "Designing unimodular sequence sets with good correlations—including an application to mimo radar," *IEEE Trans. Signal Process.*, vol. 57, no. 11, pp. 4391–4405, Nov 2009.

[9] J. Song, P. Babu, and D. P. Palomar, "Sequence set design with good correlation properties via majorization-minimization," *IEEE Trans. Signal Process.*, vol. 64, no. 11, pp. 2866–2879, 2016.

[10] Y. Li and S. A. Vorobyov, "Fast algorithms for designing unimodular waveform(s) with good correlation properties," *IEEE Trans. Signal Process.*, vol. 66, no. 5, pp. 1197–1212, March 2018.

[11] S. Rao and A. V. Mani, "Interference characterization in fmcw radars," in *Proc. IEEE Radar Conf.*, Sep. 2020, pp. 1–6.

[12] G. M. Brooker, "Mutual interference of millimeter-wave radar systems," *IEEE Trans. Electromagn. Compat.*, vol. 49, no. 1, pp. 170–181, Feb 2007.

[13] S. Sun, A. P. Petropulu, and H. V. Poor, "Mimo radar for advanced driver-assistance systems and autonomous driving: Advantages and challenges," *IEEE Signal Process Mag.*, vol. 37, no. 4, pp. 98–117, July 2020.

[14] Y. Kamiya and O. Besson, "Interference rejection for frequency-hopping communication systems using a constant power algorithm," *IEEE Trans. Commun.*, vol. 51, no. 4, pp. 627–633, April 2003.

[15] F. Uysal, "Phase-coded fmcw automotive radar: System design and interference mitigation," *IEEE Trans. Veh. Technol.*, vol. 69, no. 1, pp. 270–281, Jan 2020.

[16] X. Zhao, Y. Li, and R. Tao, "Design of single unimodular waveform with good correlation level via phase optimizations," in *Proc. 30th European Signal Process. Conf. (EUSIPCO)*, Aug 2022, pp. 1896–1900.

[17] R. Amar, M. Alaee-Kerahroodi, P. Babu, and B. S. M. R., "Designing interference-immune doppler-tolerant waveforms for radar systems," *IEEE Trans. Aerosp. Electron. Syst.*, vol. 59, no. 3, pp. 2402–2421, June 2023.

[18] M. Song, J. Lim, and D.-J. Shin, "The velocity and range detection using the 2d-fft scheme for automotive radars," in *Proc. 4th IEEE Int. Conf. Netw. Infrastructure Digit. Content*, 2014, pp. 507–510.